ELSEVIER

Applied Mathematical Modelling 22 (1998) 1047–1057

APPLIED MATHEMATICAL MODELLING

Chaotic mixing simulations

B.T. Tan *, P. Morris, M.C. Thompson, K. Hourigan

F.L.A.I.R., Department of Mechanical Engineering, Monash University, Wellington Road, Clayton, Victoria 3168, Australia

Received in revised form 21 January 1998; accepted 26 February 1998

Abstract

Numerical simulations of high Reynolds number flows in the unit driven cavity have been performed. The system is shown to become unsteady at $Re = 8125$ and chaotic at $Re = 17{,}000$. In between this range the system switches between periodic and quasi-periodic states with step-wise changes in period. A passive concentration field and passive tracer particles are introduced into the flow at its asymptotic state to show the effects of chaos on mixing. © 1998 Elsevier Science Inc. All rights reserved.

Keywords: Driven cavity; Mixing; Transition; Chaos

1. Introduction

Mixing of fluids is important in many industrial and environmental situations, but because the process is poorly understood, most studies are 'postdictive' rather than predictive. Improving efficiency is obviously an industrial imperative as costs increase with power input and length of time required for fluids to be sufficiently mixed. However, in any generalised case, many factors can be changed individually or in combination, and it is the identification of the dominant factors and modifications which lead to greater mixing efficiency.

Although full mixing vessel designs can now be studied numerically, there are still advantages in gaining an understanding at a basic level and to use this knowledge to suggest improvements. In the current study, most of the geometrical detail has been removed, and the mixing properties of the system are examined as the governing parameters are altered. Driven cavity flow can be thought of as generic mixing flow, since one of the walls provides a shearing force resulting in mechanical agitation or stirring of the fluid. Even within such a simple system however, four distinct flow regimes have been found. The transition from steady to chaotic flow, and behaviour in between, have been examined in detail, thus providing information on how mixing is affected by modifications to parameters governing the system.

The driven cavity problem consists of a unit two-dimensional square cavity with the top wall driven at a prescribed velocity, with the other three remaining stationary. This flow is a well known test problem is computational fluid dynamics, and a complete set of steady

* Corresponding author. Fax: +61 3 9905 9639; e-mail: bttanz@kutta.eng.monash.edu.au.

0307-904X/98/$ – see front matter © 1998 Elsevier Science Inc. All rights reserved.
PII: S0307-904X(98)10041-0

solutions at low Reynolds number ($\mathrm{Re} \leqslant 10{,}000$) have been obtained previously by Ghia et al. [1] which concentrated on vortex dynamics. Many previous studies have used this problem to benchmark computational schemes [2–4]. This study aims to extend the solutions to time-dependent flows at higher Reynolds number where the flow may be periodic, quasi-periodic or chaotic.

Since a global spectral expansion is being used in the numerical scheme, in order to preserve spectral accuracy the speed of the top wall is not constant as in previous studies, but approaches zero smoothly at the corners. This modified problem is sometimes referred to as "regularised driven-cavity flow" [5]. This avoids a discontinuity in the vorticity profile, and hence problems with pressure boundary conditions [6]. Suggestions for the analytic form can be found in Shen [6], where he solved the driven cavity up to $\mathrm{Re} = 16{,}000$ with a quartic profile ($u = 16x^2(1-x)^2$) for the moving lid. The solution was steady up to $\mathrm{Re} = 10{,}000$, and between $\mathrm{Re} = 10{,}500$ and 15,000, the solution appeared to be periodic with one distinct frequency. This was shown by plots of total kinetic energy and velocity at arbitrary locations as a function of time and was attributed to a Hopf bifurcation in the interval (10,000, 10,500]. The system becomes quasi-periodic with two distinct frequencies above $\mathrm{Re} = 15{,}500$; this was attributed to another bifurcation between (15,000, 15,500]. Velocity profiles which are closer to uniform can be expected to lower these values; for example Liffman [7] observed a quasi-periodic behaviour at $\mathrm{Re} = 10{,}000$ with a constant lid profile that exponentially decays at the edges ($u = 1 - \exp(-20(1-x^2))$). Verstappen et al. [8] analysed the time series of energy in the system and concluded that it is chaotic at $\mathrm{Re} = 22{,}000$.

The aim of this paper is to characterise the flow regimes as the Reynolds number is increased from initial unsteadiness to chaos. Using a passive concentration field and passive tracer particles, it will be shown that there is an improvement in mixing in the chaotic regime. The mathematical formulation and the boundary conditions will be presented in Section 2. In Section 3, the numerical scheme will be described including the spatial and temporal discretisation. The different flow regimes, the methods used to determine chaotic behaviour and the effects on mixing will be described in Section 4.

2. Mathematical formulation

The formulation is based on the non-dimensionalised incompressible Navier–Stokes equations, namely:

$$\frac{\partial \mathbf{u}}{\partial t} = -(\mathbf{u}\cdot\nabla)\mathbf{u} - \nabla p + \frac{1}{\mathrm{Re}}\nabla^2\mathbf{u} \quad \text{in } \Omega, \tag{1}$$

$$\nabla\cdot\mathbf{u} = 0 \quad \text{in } \Omega. \tag{2}$$

The two dimensional unit cavity has three stationary boundaries and a 'driving' lid with a fixed velocity

$$\mathbf{u} = ((1-\exp(-20(1-x^2)))^3, 0). \tag{3}$$

The lid profile used is similar to that used by Liffman [7], but modified to ensure that both the first derivative and second derivative are continuous at the corners. This profile is used because it is a reasonable approximation to the uniform lid driven cavity, and eliminates the corner singularities. The initial flow velocity is set to be zero throughout the domain. Ramping up the lid smoothly in time or impulsively starting it does not effect the final flow state.

A passive concentration field and passive tracer particles are used to observe mixing in the flow. The former is governed by a nondimensional advection–diffusion equation [9],

$$\frac{\partial c}{\partial t} = -(\mathbf{u}\cdot\nabla)c + \frac{1}{\mathrm{Pe}}\nabla^2 c \quad \text{in } \Omega \tag{4}$$

with a vanishing concentration flux on the solid boundaries,

$$\mathbf{n}\cdot\nabla c = 0 \quad \text{on } \Gamma. \tag{5}$$

In this closed domain, conservation arguments demand that the spatial integral of the concentration field remains constant in time. Therefore the condition to remove the non-uniqueness caused by the arbitrary additive constant in the solution of Eqs. (4) and (5) is

$$\int_{\Omega} c \, \mathrm{d}A - \int_{\Omega} c_0 \, \mathrm{d}A = 0, \tag{6}$$

where c_0 is the initial concentration field. In the current work, this is given by

$$c_0(x,y) = \exp(-20((x-0.75)^2 + (y-0.25)^2)) \quad \text{in } \Omega \tag{7}$$

which provides a concentrated circular region centered at (0.75, 0.25) with a peak concentration of 1.0. The diffusivity of the concentration field and the flow field are chosen to be equal ($\mathrm{Pe} = \mathrm{Re}$).

The passive particles are convected with the velocity field. The governing equations that advances these particles in time are:

$$\frac{\mathrm{d}x}{\mathrm{d}t} = u, \quad \frac{\mathrm{d}y}{\mathrm{d}t} = v. \tag{8}$$

Initially, 150×150 particles are evenly placed within a 0.2 units square box centered at the same location as the initial passive concentration field as shown in Fig. 5(a). Therefore these initial conditions are slightly different to those used in the passive concentration field simulations.

3. Numerical technique

Previous mixing simulations [10] have demonstrated that false predictions of mixing may result from numerical errors, especially in the chaotic regime. To minimise such errors, the spatial variables are handled by a high-order spectral expansion. As the flow is wall bounded, Chebyshev polynomials [11] are used in each direction within the flow. This is advantageous because of the natural compression of the grid around the bounding walls. Although a Fast Fourier Transform can be used for derivative calculations, direct multiplication using optimised matrix routines are faster [5]. The increase in floating point operations is offset by the logical operations necessary for the transform method. Implicit steps are solved using a matrix diagonalisation technique [11].

The time stepping scheme is a modified version of the three-step operator-splitting method used for previous spectral element simulations [6]. The modifications are necessary to facilitate the use of a Runge–Kutta scheme for the convection term. Since the derivatives in the Navier–Stokes equations have no explicit dependence on t, a memory efficient Runge–Kutta scheme can be used [11]. The pressure is solved implicitly and the diffusion treated with a Crank–Nicholson scheme. The algorithm for the modified scheme is:

Set $\mathbf{u} = \mathbf{u}^n$

For $k = s, 1, -1$

$$\frac{\mathbf{u}^* - \mathbf{u}^n}{\Delta t/k} = -\mathbf{u} \cdot \nabla \mathbf{u},$$

$$\frac{\mathbf{u}^{**} - \mathbf{u}^*}{\Delta t/k} = -\nabla p, \qquad \nabla \cdot \mathbf{u}^{**} = 0,$$

$$\frac{\mathbf{u} - \mathbf{u}^{**}}{\Delta t/k} = \frac{1}{2\mathrm{Re}}(\nabla^2 \mathbf{u} + \nabla^2 \mathbf{u}^n).$$

End for

Set $\mathbf{u}^{n+1} = \mathbf{u}$

with s the order of the Runge–Kutta scheme. Fourth order ($s = 4$) is used for all simulations.

The passive concentration field is solved on the same mesh as the Navier–Stokes equations. A similar operator-splitting technique is used for the passive concentration field. The algorithm is:

Set $c = c^n$

For $k = s, 1, -1$

$$\frac{c^* - c^n}{\Delta t/k} = -\mathbf{u}^{n+1} \cdot \nabla c,$$

$$\frac{c - c^*}{\Delta t/k} = \frac{1}{2\mathrm{Pe}}(\nabla^2 c + \nabla^2 c^n).$$

End for

Set $c^{n+1} = c$.

For the passive particle simulations, the velocities at the particle positions are found by a second-order Taylor expansion from the nearest nodes using the derivatives calculated by the spectral scheme. A fourth-order Runge–Kutta scheme is used to advance the particles at each time step.

The time variation of the total kinetic energy can be used to provide information on the state of the flow. This method has been used previously for studying this problem [5,7]. The total kinetic energy is given by

$$E(n\Delta t) = \frac{1}{2}\sum_{j=0}^{M-1}\sum_{i=0}^{N-1} A_{ij}[(u_{ij}^n)^2 + (v_{ij}^n)^2], \tag{9}$$

where the weighing factors A_{ij} are local cell areas at the point (x_i, y_j).

4. Results and discussion

4.1. Flow regimes

The simulations were carried out with 80 nodes in each direction, and $\Delta t = 0.0025$ time units. A steady solution results for $\mathrm{Re} \leqslant 8{,}000$. This was obtained after a long settling time of approximately 5000 time units, where the fluctuations in kinetic energy were less than 0.0001% and the fluctuations in velocity were of the same order as the numerical error. Poliashenko and Aidun [12] analysed a driven cavity with a uniform profile lid using an eigenvalue analysis and found the

first bifurcation to be at Re = 7763. This difference of a few percent is most likely due to the slight difference in the top wall boundary condition.

Between Re = 8125 and 9750, the temporal variation of the total kinetic energy shows that the system appears to be perfectly periodic, with a period of approximately 2.25 time units. The mean kinetic energy decreases linearly in this range with increasing Reynolds number. This is similar to the observation by Shen [5] in the first bifurcation region of the regularised driven cavity. The decrease in mean total kinetic energy also extends to higher Reynolds numbers as shown in Fig. 1.

Simulations were then performed at increasing Reynolds number. At Re = 10,000 and 11,000, the system exhibits a quasi-periodic state with two dominant frequencies. The dominant periods at Re = 10,000 are 2.32 and 3.85, and are 3.76 and 6.40 at Re = 11,000. Shen [5] also observed a two-periodic state when the Reynolds number increased past the perfectly periodic regime. The plot of kinetic energy at Re = 10,000 as a function of time is very similar to that obtained by Liffman [7].

The system appears to settle down to one frequency between Re = 12,000 and 13,000 with a period of oscillation of 1.47. At Re = 14,000 and 14,500, another quasi-periodic regime with dominant periods of 1.52 and 15.06 is observed. The system again settles down to a periodic cycle at Re = 15,000 and 15,500 with a period of 1.56. Fig. 1 shows the kinetic energy trace at several Reynolds numbers illustrating the switching between periodic to quasi-periodic states. The stepwise change in periods is summarised in Fig. 2. From Re = 15,750 onwards, there is an increase in the number of modes especially at longer periods shown by the spectral plots in Fig. 3. This then leads to broad spectral features characteristic of chaos detectable at Re = 17,000 and 20,000.

Each simulation is integrated until the total kinetic energy reached an asymptotic state. For the periodic states, the sinusoidal signal is ensured to be symmetrical for at least 50 cycles. In the quasi-periodic and chaotic states, the requirements are that the mean is constant and the Fourier transform of the kinetic energy signal is constant when taken over several time periods. This would typically require several thousand time units. To reduce the integration time to a manageable level, the solution at the next lower Reynolds number is used to provide initial conditions for the simulations. Observations of fluctuations of velocity components at arbitrary locations in

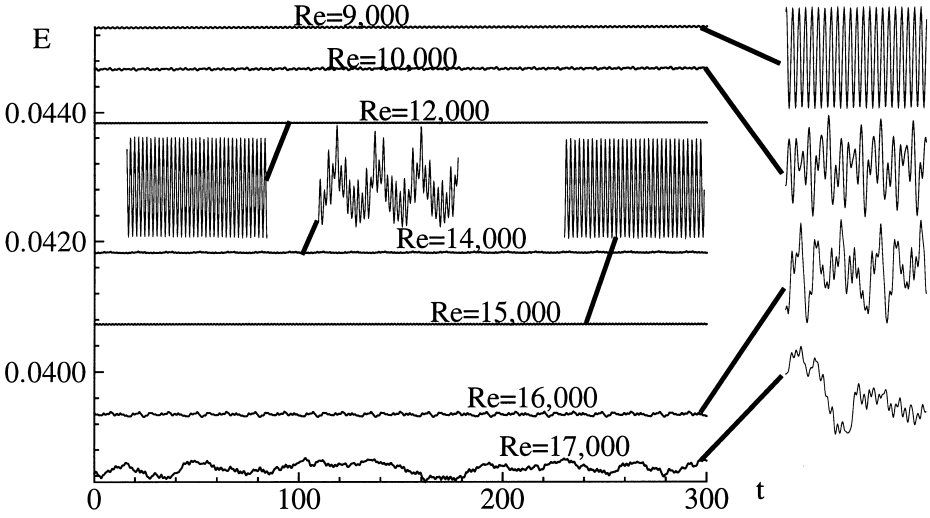

Fig. 1. Total kinetic energy trace for 300 time units at several Reynolds numbers. Traces are taken when an asymptotic state has been reached. Inserts show 50 time units of detailed behaviour at each Re.

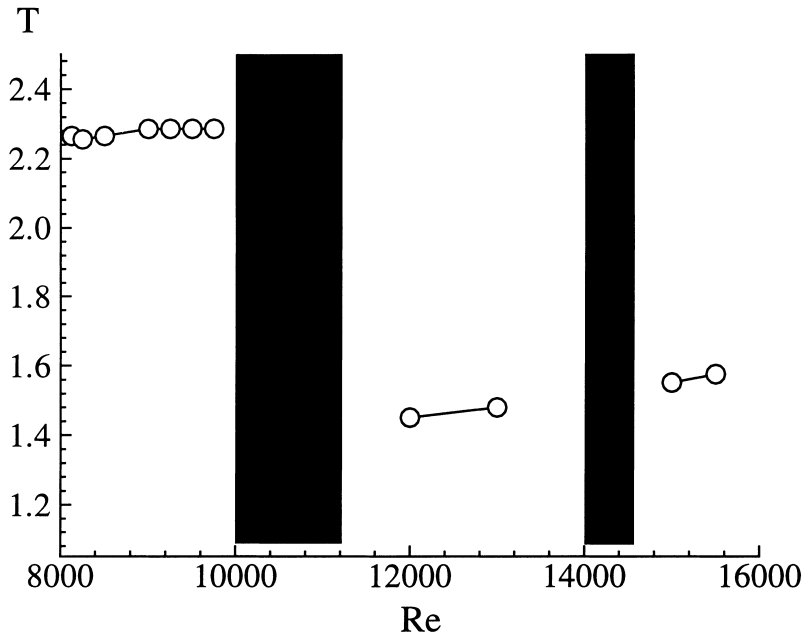

Fig. 2. Period of oscillation as a function of Reynolds number. Shaded regions exhibit quasi-periodic behaviour.

the cavity show similar behaviour to the total kinetic energy. To ensure that the results were grid independent, additional simulations were carried out at a resolution of 100 nodes in each direction at Re = 14,000, 17,000 and 20,000. The features in the flow field and the behaviour of the total kinetic energy were consistent with the lower resolution simulations.

4.2. Test for chaos

Once the flow has reached an asymptotic state, the velocity field is perturbed slightly. The perturbed and unperturbed fields are then integrated forward in time. The L2 norm of the difference in velocity fields is measured as a function of time to determine if the solutions diverge exponentially. This is typical of chaotic type behaviour [13]. The perturbed velocity field is of the form

$$\mathbf{u}' = \mathbf{u} + \epsilon f(x,y). \tag{10}$$

The size of the perturbation is chosen to be small, $\epsilon = 0.0001$, and $f(x,y)$ is chosen so that the resultant flow field satisfies both the boundary conditions and continuity. Here it is chosen to be

$$\begin{aligned} f(x,y) =& (2.0\ \sin(2\pi x)\ \cos(2\pi x)\ \sin^2(2\pi y), \\ & -2.0\ \sin(2\pi y)\ \cos(2\pi y)\ \sin^2(2\pi x)) \quad \text{in} \quad \Omega. \end{aligned} \tag{11}$$

The initial L2 norm was 4.2736×10^{-7}.

This test was done at Re = 10,000, 17,000 and 20,000. At Re = 10,000, the L2 norm between the two solutions remained at the same level as the initial value. After 200 time units there was no indication of divergence. At Re = 17,000, the solutions initially remained close (L2 norm remained of the same order), but after 50 time units the solutions rapidly diverged to different states. The L2 norm increased by several orders of magnitude in this time. This was also the case at

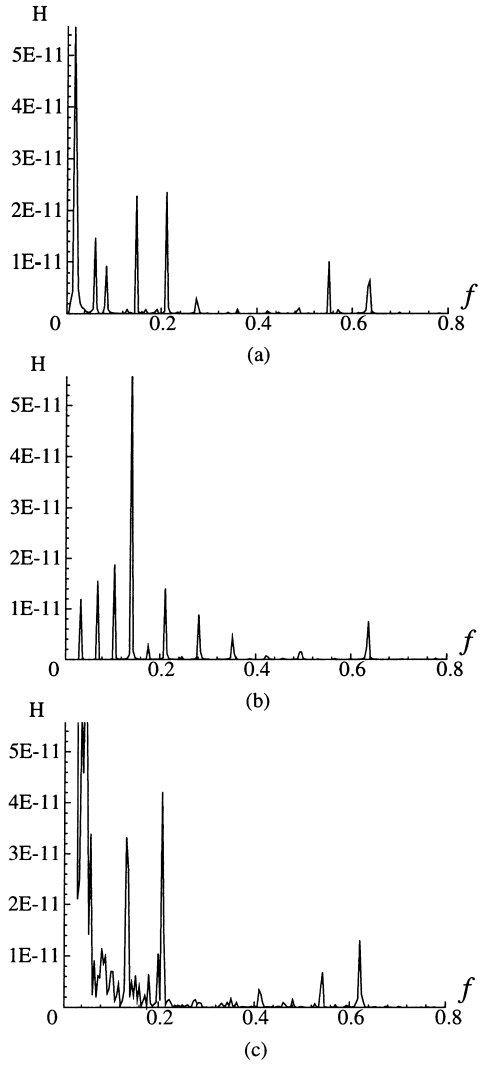

Fig. 3. Spectral plot of kinetic energy at: (a) Re = 15,750; (b) Re = 16,000; (c) Re = 17,000 showing increasing spectral modes at the transition to chaos.

Re = 20,000, but the solutions started diverging rapidly 40 time units after the perturbations were introduced. Therefore the solutions at Re = 17,000 and 20,000 exhibit chaotic features.

4.3. Passive concentration field

Once the flow has reached an asymptotic state, the initial condition for the passive concentration field is introduced. The simulations were then integrated forward 50 time units allowing the passive concentration field to be convected and diffused with the flow field. The concentration contours for Re = 8000, 10,000, 14,000, 17,000 and 20,000 are shown in Fig. 4. At Re = 8000 and 10,000, the passive concentration field is convected with the cavity circulation and the mixing is dominated by diffusion. There is less diffusion of the concentration field at Re = 14,000, 17,000 and 20,000. The distortions to the contour lines at Re = 17,000 can be attributed to the chaotic nature of the flow. At Re = 20,000, there is significantly more stretching and distortion of the

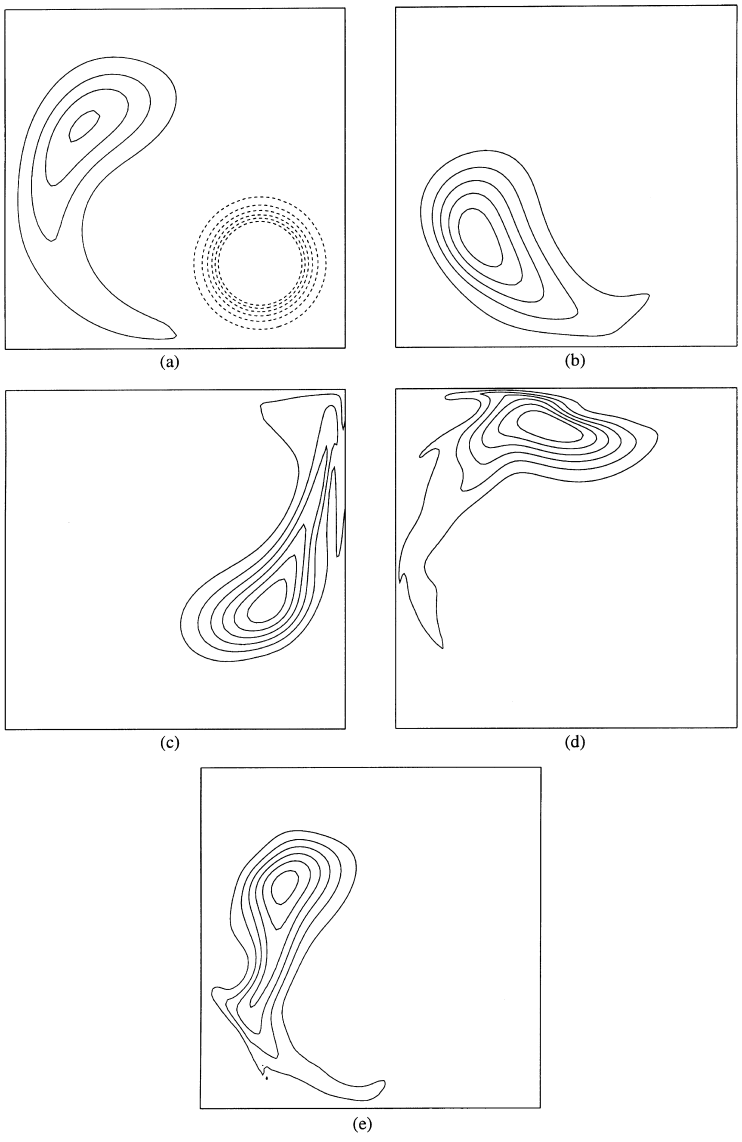

Fig. 4. Contours of passive concentration field 50 time units after introduction to the asymptotic flow state at: (a) Re = 8000; (b) Re = 10,000; (c) Re = 14,000; (d) Re = 17,000; (e) Re = 20,000. Contour levels are at 0.05, 0.10, 0.15, 0.20, 0.25 and 0.30. The 'driving' lid is at the top and the direction is towards the right of the page. Dashed lines in (a) represent the initial scalar field.

passive concentration field. This indicates that in the chaotic region, convective forces will stretch and distort the fluid perhaps resulting in enhanced mixing. The concentration field at lower Reynolds number is more diffused because it diffuses at the same rate as the flow (Pe = Re) but mixing, which involves distortions of the fluid, is more evident in the chaotic regime.

4.4. Passive tracer particles

A similar process is undertaken with the passive tracer particles. After 50 time units of integration, the final positions of the particles are shown in Fig. 5. Although for each simulation the

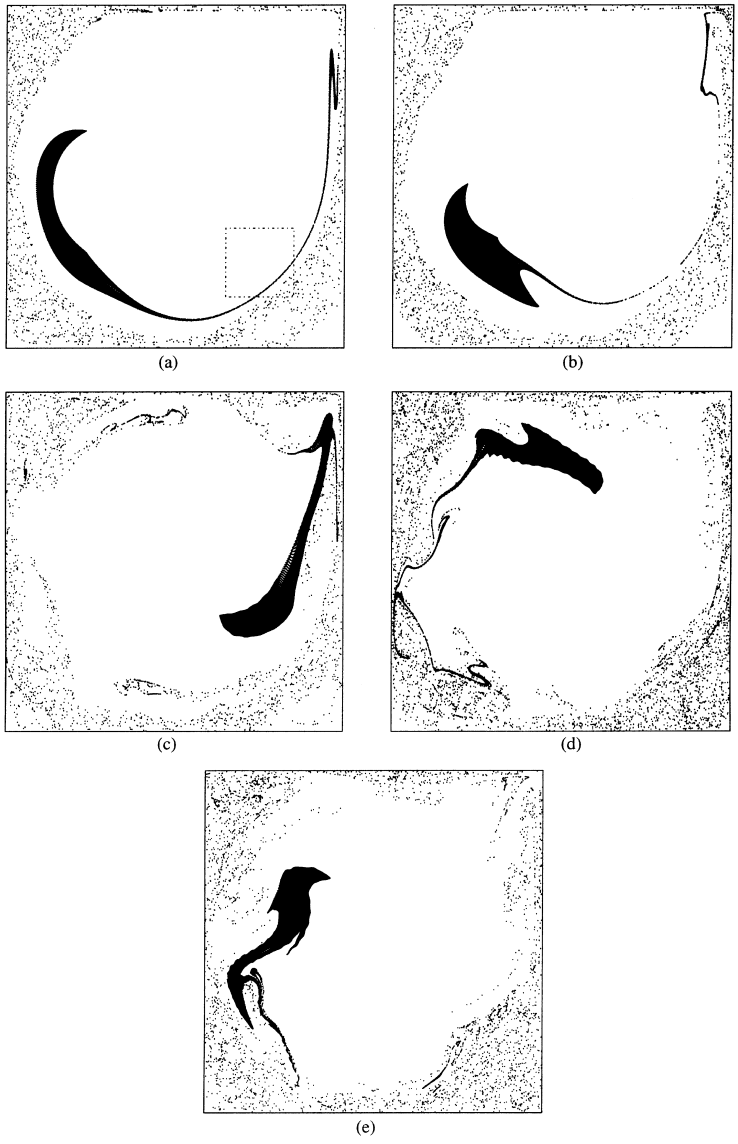

Fig. 5. Position of passive tracer particles 50 time units after introduction to the asymptotic flow state at: (a) $Re = 8000$; (b) $Re = 10{,}000$; (c) $Re = 14{,}000$; (d) $Re = 17{,}000$; (e) $Re = 20{,}000$. The 'driving' lid is at the top and the direction is towards the right of the page. Particles were initially placed uniformly distributed in a square area shown by the dashed lines in (a).

majority of the particles still remain close together over these short time periods, for the chaotic cases, there is some kinking and distortions of the convected clumps. In particular the 'tails' of the clumps also show the characteristic stretching and folding behaviour of chaotic transport.

5. Conclusions

The driven cavity, in this case, was found to be steady until $Re = 8000$. Between $Re = 8125$ and 15,500, the flow switches between a periodic and a quasi-periodic state with a step-wise decrease in

period with increasing Reynolds number. For $Re \leqslant 15{,}750$, the number of modes increase rapidly until the system becomes chaotic at approximately $Re = 17{,}000$.

Once the flow has reached an asymptotic state, a small perturbation introduced to the solutions at $Re = 17{,}000$ and 20,000 caused the system to diverge exponentially from the unperturbed state. This is typical of chaotic behaviour where initially small changes are amplified exponentially with time. There is some enhancement of mixing in the chaotic regime by stretching and distortion of fluid elements.

Nomenclature

A	area
c	passive concentration field
c_0	initial passive concentration field
p	pressure
Pe	Peclet number
Re	Reynolds number
t	dimensionless time
$\mathbf{u}$	velocity vector
$\mathbf{u}^*, \mathbf{u}^{**}$	intermediate velocity vector
$\mathbf{u}'$	perturbed velocity vector
ϵ	small constant

Acknowledgements

The first author (B.T.T.) acknowledges the financial support of an Overseas Postgraduate Research Scholarship and a Monash Graduate Scholarship. The granting of computing time from the Monash High Performance Computer facility that allowed the simulations to be performed is gratefully acknowledged.

References

[1] U. Ghia, K.N. Ghia, C.T. Shin, High-Re solutions for incompressible flow using the Navier-Stokes equations and a multigrid method, J. Comp. Phys. 48 (1982) 387–411.
[2] G. Comini, M. Manzan, C. Nonino, Finite element solution of the streamfunction-vorticity equations for incompressible two-dimensional flows, Int. J. Num. Methods Fluids 19 (1994) 513–525.
[3] E. Weinan, J. Liu, Essentially compact schemes for unsteady viscous incompressible flows, J. Comp. Phys. 126 (1996) 122–138.
[4] S. Hou, Q. Zou, S. Chen, G. Doolen, A.C. Cogley, Simulation of cavity flow by the lattice boltzmann method, J. Comp. Phys. 118 (1995) 329–347.
[5] J. Shen, Hopf bifurcation of the unsteady regularized driven cavity flow, J. Comp. Phys. 95 (1991) 228–245.
[6] G.E. Karniadakis, M. Israeli, S.A. Orszag, High-order splitting methods for the incompressible Navier-Stokes equations, J. Comp. Phys. 97 (1991) 414–443.
[7] K. Liffman, Comments on a collocation spectral solver for the helmholtz equation, J. Comp. Phys. 128 (1996) 254–258.
[8] R. Verstappen, J.G. Wissink, A.E.P. Veldman, Direct numerical simulation of driven cavity flows, App. Sci. Res. 51 (1993) 377–381.
[9] V. Toussaint, P. Carriere, F. Raynal, A numerical Eulerian approach to mixing by chaotic advection, Phys. Fluids 7 (11) (1995) 2587–2600.

[10] A. Souvaliotis, S.C. Jana, J.M. Ottino, Potentialities and limitations of mixing simulations, AIChE 41 (1995) 1605–1621.
[11] C. Canuto, M.Y. Hussaini, A. Quarteroni, T.A. Zang, Spectral methods in fluid dynamics, Springer, Berlin, 1988.
[12] M. Poliashenko, C.K. Aidun, A direct method for computation of simple bifurcations, J. Comp. Phys. 121 (1995) 246–260.
[13] E.N. Lorenz, Deterministic nonperiodic flow, J. Atmospheric Sci. 20 (1963) 130–141.